

**Hole burning and higher-order photon effects in attosecond light-atom interaction**P. L. Price,<sup>1,\*</sup> L. D. Noordam,<sup>2</sup> H. B. van Linden van den Heuvell,<sup>2</sup> and F. Robicheaux<sup>1,†</sup><sup>1</sup>*Department of Physics, Auburn University, Auburn, Alabama 36849, USA*<sup>2</sup>*Institute of Physics, University of Amsterdam, Post Office Box 94485, 1090GL Amsterdam, The Netherlands*

(Received 10 January 2014; published 13 March 2014)

We have performed calculations of attosecond laser-atom interactions for laser intensities where interesting two- and three-photon effects become relevant. In particular, we examine the case of “hole burning” in the initial orbital. Hole burning is present when the laser-pulse duration is shorter than the classical radial period because the electron preferentially absorbs the photon near the nucleus. We also examine how the three-photon Raman process can lead to a time delay in the outgoing electron for the energy near one-photon absorption. For excitation out of the hydrogen  $2s$  state, an intensity of  $2.2 \times 10^{16}$  W/cm<sup>2</sup> leads to a 6-as delay of the outgoing electron. We argue that this delay is due to the hole burning in the initial state.

DOI: [10.1103/PhysRevA.89.033414](https://doi.org/10.1103/PhysRevA.89.033414)

PACS number(s): 32.80.Fb, 78.47.J–, 32.80.Rm

**I. INTRODUCTION**

The past several decades have witnessed an increase in the speed of lasers as tracked by the duration of a laser pulse. In recent years, experimental groups have been able to decrease this duration into the attosecond regime [1]. With each decrease in duration of the laser pulse, it is possible to probe quantum systems on shorter time scales. For example, there have been many recent measurements and calculations of the delay in the photoionization of electrons from atoms [2–5]. This example is interesting in that the delay is only of order 10 as but can be measured using a streaking infrared field *and* in that measurements and calculations differ in the expected delay; the reason for the difference is not clarified. One of the results we discuss below is that delays in electron ejection naturally occur at higher laser intensities.

Although both the laser frequency and duration determine what types of systems and phenomena are best investigated, there are types of processes whose similarities extend from the attosecond to the picosecond regime. One of the processes that spans a broad regime is that in which a short laser pulse can burn a hole in a wave function. The reason is that photoabsorption is often highly position dependent. For example, stationary phase considerations lead to the realization that photoionization occurs near the nucleus within a region  $r \sim \sqrt{(\ell + 1)/\omega}$ , with  $\omega$  being the angular frequency of the laser [6,7]. Thus, a laser pulse that is shorter than the radial period of the electron can deplete the wave function in the neighborhood of the nucleus [8].

Figure 1 is a schematic of two-photon processes. The gray bands are meant to indicate the spread in energy for the processes that arise from the short duration of the laser. The dark arrow is the one-photon excitation step. The narrow solid arrows are the two-photon absorption (for increasing energy) and the Raman process (for decreasing energy). The Raman process back to  $\ell = 0$  gives the hole burning of the initial wave function. The dashed arrows indicate the three-photon

process that can interfere with the one-photon absorption; the three-photon processes can modify both the energy distribution and the ejection time of the electron.

Hole burning was investigated in Rydberg states where the radial period can be in the picosecond regime [9,10]. For a state with energy  $E = -1/2\nu^2$ , the radial period is given by  $T_{\text{Ryd}} = 2\pi\nu^3$  a.u., which is  $T_{\text{Ryd}} = 1.52 \times 10^{-4}\nu^3$  ps. Thus, states with  $\nu > 18.7$  have periods longer than 1 ps. One of the manifestations of hole burning is that of Raman transitions to nearby states with the same  $\ell$ . One way to think of this connection is that the wave function with the hole,  $\psi_h$ , is projected onto the eigenstates with the laser off. Since the  $\psi_h$  mostly resembles the initial state and has the same angular momentum, the projection onto the initial state and states with small change in  $\nu$  and no change in  $\ell$  will be emphasized [8]. The size of the hole in space increases with the duration of the laser pulse because the depleted part of the wave function moves to larger  $r$  and the wave function at larger  $r$  moves to smaller  $r$  where it can be depleted by the laser; Fig. 3 of Ref. [9] shows that short pulses only deplete the wave function at small  $r$  while a laser pulse longer than the Rydberg period depletes the wave function uniformly at all  $r$ . Thus, a short laser pulse will lead to a wider energy range of final states. An equivalent statement in the frequency domain is that short pulses have a large bandwidth, supporting Raman transfer to neighboring states.

In this paper, we examine the phenomenon of hole burning in the regime of attosecond laser pulses. Since hole burning is at least a two-photon process, the intensity regime will be higher than what is currently experimentally achieved but not so high that experiments are unthinkable. While the basic phenomenon of hole burning should be the same, there are differences due to the shorter time scale and hence the lower states involved. One difference is that for Rydberg states and picosecond lasers the hole burning leads to population at both higher and lower energies (the principle quantum number can both increase or decrease) while for attosecond lasers the initial state is usually the ground state so population can only transfer to higher energies. Another difference is that the experiments on Rydberg state hole burning did not investigate when the *ejected* electron is modified by the hole burning. In attosecond physics, the time delay of the ejected electron [2–5] is often one of the more interesting parts of the

\*Now at Physics Department, University of Connecticut, 2152 Hillside Rd., Storrs, Connecticut 06269-3046, USA

†Now at Department of Physics, Purdue University, West Lafayette, Indiana 47907, USA; robichf@purdue.edu

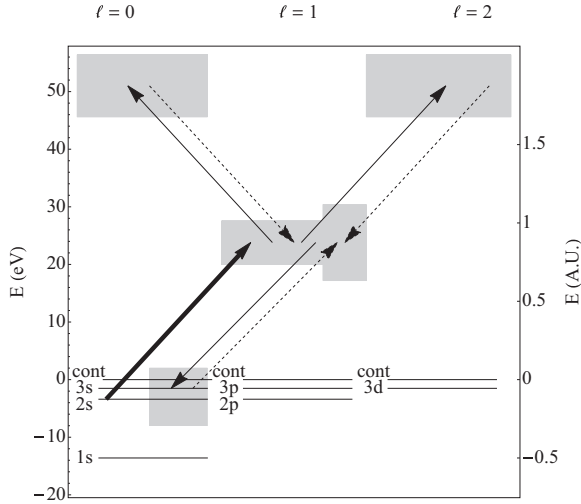


FIG. 1. A schematic drawing of the energy levels and transitions described in the paper.

measurement but also used to define the “zero” time delay in pump-probe experiments. We give calculations for this process and show that the hole burning leads to a delay in the ejection of the electron. This effect arises from the interference between one-photon absorption and a three-photon process (two absorptions and one emission). Since the time delay from hole burning requires higher intensity, we do not think it is an explanation of the discrepancy between the measured and calculated delays [2–5].

The term “hole” is used in many different contexts. Unless we clearly state otherwise, the term “hole” will mean that the wave function has a region in *space* where  $|\psi|^2$  is smaller than for the original wave function (Fig. 5 of Ref. [8]). For the process discussed in this paper, the laser makes a hole in the wave function at small  $r$  if the laser duration is much shorter than the period associated with that state. Thus, defining  $\psi_0$  to be the wave function just *before* the laser interacts with the atom and  $\psi(r, t)$  to be the wave function just *after* the laser interacts with the atom, the quantity  $|\psi_0(r)|^2 - |\psi(r, t)|^2$  would be nonzero and positive only for  $r$  small compared to the  $\langle \psi_0 | r | \psi_0 \rangle$ .

We use atomic units unless the International System of units is explicitly given.

## II. NUMERICAL METHOD

We solved the time dependent Schrödinger equation by representing the wave function on a grid of radial points and an angular momentum basis. A more extensive discussion of the technique can be found in Ref. [11]. In our calculations, we used linearly polarized light which leads to a wave function that can be represented by the summation

$$\Psi(\vec{r}) = \sum_{\ell} [R_{\ell}(r, t)] Y_{\ell m}(\Omega), \quad (1)$$

where the radial functions,  $R_{\ell}$ , contain all of the useful information about the wave function. The maximum  $\ell$  in the sum is determined by the duration, strength, and frequency of the laser and was chosen so that less than  $10^{-9}$  of the

population was in  $\ell_{\max}$ . For ease in solving the time dependent Schrödinger equation, we consider the Hamiltonian for this calculation as the sum of two terms:

$$H = H_1 + H_2 = H_{\text{atom}} + H_{\text{field}}, \quad (2)$$

where  $H_1$  is the atomic Hamiltonian which contains the kinetic-energy operator and the spherical potential from the electron-ion interaction and the  $H_2$  is the laser-electron interaction. For hydrogen, the electron-ion potential is simply  $-1/r$ . For the other atoms presented in this paper, a model potential can be used.

The Hamiltonian for the laser field was taken to be in the length gauge. We do not need to worry about the increasing size of the laser potential with  $r$  because the laser duration is so short the electron does not travel far before the laser intensity returns to zero. We chose  $H_2 = zE(t)$  where  $E(t) = -dA/dt$  with

$$A(t) = F(t) \frac{1}{\omega_0} \sin(\omega_0 t + \phi). \quad (3)$$

The  $\phi$  is the carrier envelope phase and  $F(t)$  is a smooth function giving the envelope. We chose this to be a Gaussian  $F(t) = F_{\max} \exp(-t^2/t_w^2)$  with  $F_{\max}$  being the maximum electric field when the carrier envelope phase is zero.

We used a split operator method with a Crank-Nicolson approximation to step the wave function by  $\delta t$ . The approximation is

$$\Psi(t + \delta t/2) = U_2(t, \delta t/2) U_1(\delta t) U_2(t, \delta t/2) \Psi(t - \delta t/2), \quad (4)$$

where

$$U_j(t, \delta t) = [1 - i H_j(t) \delta t/2] [1 + i H_j(t) \delta t/2]^{-1} \quad (5)$$

gives  $O(\delta t^3)$  accuracy for one time step. In the propagator, we only need to perform the  $U_2$  when  $|t| < 6t_w$  because  $H_2$  is approximately zero outside of that range. Both the  $H_1$  and  $H_2$  operators can be represented as tridiagonal matrices. For the electric field, the operator  $H_2$  only couples  $\ell$  to  $\ell \pm 1$ . We used two approximations for  $H_1$ , both of which give a tridiagonal representation, as a test of convergence. In the simplest approximation, we used equally spaced points in  $r$  (i.e.,  $r_j = j\delta r$ ) and a three point difference for the radial kinetic energy. The more complicated approximation used a square-root mesh and a Numerov approximation as in Ref. [12]. In all calculations, we checked convergence with respect to the number of radial points, the number of angular momenta, and the number of time steps. For the calculations presented here, we used 3000 radial points in a square-root mesh with  $r_{\max} = 350$  a.u.,  $\ell_{\max} = 13$ , and  $dt = 0.01\pi/\omega_0$  (i.e.,  $1/200$  of the laser period), although most calculations are fully converged with less stringent choices.

Before the laser turns on, the wave function is in an eigenstate. We find the eigenstate by diagonalizing  $H_1$  in a finite region  $r < r_{\max}$ . The  $r_{\max}$  is chosen to be large enough that the wave function cannot reach that distance while the laser is on. We also used the eigenstates of  $H_1$  to compute the energy distribution of the final state. The eigenstates go to zero at  $r_{\max}$ , which leads to a discretized continuum. The energy distribution is defined so that  $P(E)dE$  is the probability for the electron to be within the energy range  $E$  and  $E + dE$ . The energy distribution with angular momentum  $\ell$  is approximated

by

$$P_\ell(\bar{E}) = \frac{|\langle a+1, \ell | \Psi \rangle|^2 + |\langle a, \ell | \Psi \rangle|^2}{2(E_{a+1, \ell} - E_{a, \ell})}, \quad (6)$$

where  $E_{a, \ell}$  is the energy of the  $a$ th eigenstate with angular momentum  $\ell$ ,  $\bar{E} = (E_{a+1, \ell} + E_{a, \ell})/2$  is the average of the two energies, and  $\langle a, \ell | \Psi \rangle$  is the projection of that eigenstate on the wave function. This form is chosen because the probability for the electron to have energy between  $E_{a, \ell}$  and  $E_{a+1, \ell}$  is approximately  $P_\ell(\bar{E})\Delta E \simeq (|\langle a+1, \ell | \Psi \rangle|^2 + |\langle a, \ell | \Psi \rangle|^2)/2$  where  $\Delta E = E_{a+1, \ell} - E_{a, \ell}$ . We also use this definition for negative-energy states, which allows us to treat both positive and negative energy on the same curve. This has the disadvantage that it is not clear what is the population in an individual state, which is a measurable quantity.

### III. TWO-PHOTON PROCESSES

In this section, we present results on two-photon ionization and on one-photon absorption followed by one-photon emission (and vice versa). We investigate the latter process in more detail because it is the mechanism that leads to ‘‘hole burning’’ of the initial orbital [9]. It is important to remember that even a weak laser pulse whose time width is shorter than the Rydberg period will burn a hole in the wave function. The depth of the hole increases with laser intensity and, for weak fields, the result of the hole burning will scale with the square of the intensity [8]. However, the states described in this section are not populated by other mechanisms and, thus, can be distinguished even for weak lasers.

Figure 2 shows the energy distribution in atomic units for the two-photon processes when starting from the  $2s$  state of H. For the presentation of the energy distribution, we set the population in the  $2s$  to zero when using Eq. (6) because we

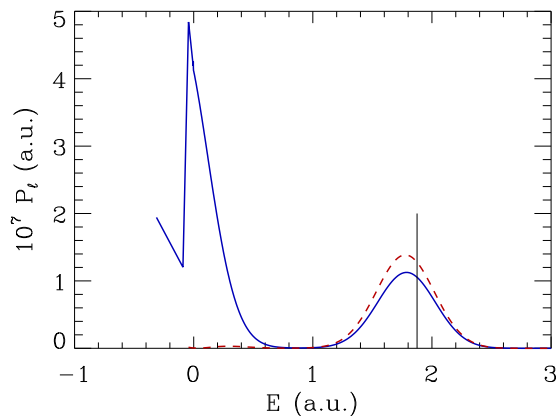


FIG. 2. (Color online) The energy distribution in atomic units of electrons for  $\ell = 0$  (solid line) and  $\ell = 2$  (dashed line). In this calculation, we set  $\omega = 1$ ,  $F_{\max} = 0.05$  a.u., and  $t_w = 6.0$  a.u. In the energy distribution formula, we set the population of the  $2s$  state to zero. The peak just below 2 a.u. is from two-photon absorption; the vertical line marks the position where a narrow-band laser would have the two-photon ATI peak. The Raman feature is from approximately  $-0.2$  to  $0.8$  a.u. The  $\ell = 2$  Raman transition is very weak and is hardly visible on the graph. The  $\ell = 0$  Raman structure is associated with hole burning in the initial state.

want a plot of what states gained population; this choice leads to an artificial dip in the Raman process. The solid line is the energy distribution where the electron has  $\ell = 0$  and the dashed curve is for  $\ell = 2$ . In this calculation, we set  $\omega = 1$  (equal to 27.2 eV,  $\lambda = 45.6$  nm),  $F_{\max} = 0.05$  a.u., and  $t_w = 6.0$  a.u. The full width at half maximum (FWHM) of the laser intensity is  $t_{\text{FWHM}} = \sqrt{2 \ln 2} t_w$ , which corresponds to 170 as in this calculation. The electric field corresponds to a maximum laser intensity of  $8.8 \times 10^{13}$  W/cm<sup>2</sup>, which is in the perturbative regime. Doubling the intensity increases the scale of Fig. 2 by a factor of 4. For this laser width, the state with the most population is the  $1s$  state; this is not obvious in Fig. 2 due to the large energy difference between the  $1s$  and  $2s$  states which gives a large denominator in Eq. (6).

There are a few features worth noting in Fig. 2. The two-photon absorption peak is at nearly the same energy for the two angular momenta. However, this energy, 1.78 a.u., is *not* at the expected energy for two-photon absorption, which is  $-1/8 + 2 = 1.875$  a.u.; the expected energy is marked by a vertical line in the graph. The peak is shifted down in energy because the two-photon absorption amplitude is a decreasing function of energy; the product of the decreasing absorption amplitude and the Gaussian centered at 1.875 a.u. gives the approximately 0.09-a.u. shift. Using a longer laser pulse leads to this feature becoming narrower in energy with the peak shifting toward the expected value of 1.875 a.u. For example, the peak shifts to 1.83 a.u. when  $t_w$  is increased to 8 a.u. In contrast to the Raman process discussed below, the two-photon absorption has nearly equal population in  $\ell = 0$  and 2.

In the  $\ell = 0$  energy distribution, plotted in Fig. 2, there is large population corresponding to the two-photon process where one photon is absorbed and one photon is emitted. This process is approximately 100 times smaller for  $\ell = 2$ . This disparity might be surprising considering that the two-photon absorption probability is comparable. The suppression of the  $\ell = 2$  population could be because the absorption and emission take place at  $r \simeq 1$  a.u.; at this radius, the  $\ell = 2$  channel is in the classically forbidden region which reduces the matrix element for this transition. We attribute the  $\ell = 0$  population to hole burning of the initial orbital. The coherent superposition of these Raman states with the initial state leads to a ‘‘hole’’ in the initial state at small  $r$ . Figure 3 shows the total probability ( $\ell = 0$ ) in the Raman transition and in the two-photon absorption as the pulse duration is increased keeping all other parameters fixed; the data in this figure come from integrating the energy distribution up to  $E = 0.875$  for the Raman transition and above  $E = 0.875$  for the two-photon absorption [13]. The dependence of the two-photon absorption on  $t_w$  in Fig. 3 is the simplest to understand. The probability is approximately proportional to the duration because the ionization continues while the pulse is on. The behavior of the Raman population is more interesting, showing a slow increase followed by a decrease. The Raman population starts decreasing when  $t_w$  is comparable to half the classical period; more specifically we find  $t_w \sim \sqrt{8 \ln 2} n^3$ . This condition is when the energy FWHM of the laser field equals  $1/n^3$ , i.e., the energy spacing of the atom. This fits with the interpretation of the Raman process with  $\Delta \ell = 0$  as equivalent to hole burning. When the laser is on for a time comparable to or longer than

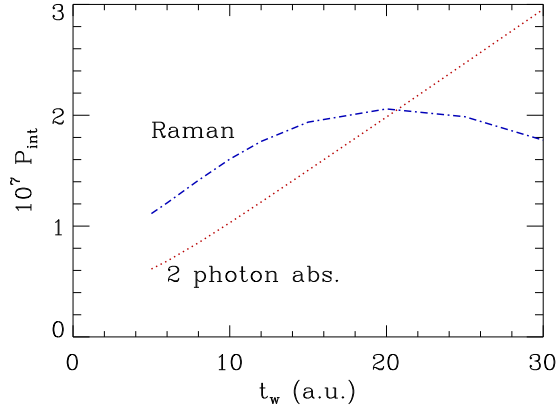


FIG. 3. (Color online) The total probability to be in the  $\ell = 0$  Raman structure (dash-dotted line) or the  $\ell = 0$  two-photon absorption peak (dotted line). All laser parameters are as in Fig. 2 except for the pulse width,  $t_w$ , which is varied. The two-photon absorption is approximately proportional to the duration of the laser pulse. The probability for Raman transition is not proportional to the pulse duration even for small  $t_w$  and begins to decrease when the bandwidth of the laser is too small to reach the  $3s$ ,  $4s$ ,  $\dots$ ,  $n$  states. As a point of comparison,  $1/(E_{3s} - E_{2s}) \simeq 14$  a.u. For pulses longer than  $\tau_{2s}$ , the bandwidth becomes insufficient to reach the  $3s$  state in a two-photon Raman process.

the radial period for the hole in the wave function, then there should not be any hole burning.

Figure 4 shows how the energy distribution for the  $\ell = 0$  Raman transition changes as the pulse duration is increased keeping all other parameters fixed. One can see that the energy width is decreasing while the peak is increasing for longer  $t_w$ . However, the longest times have almost no increase in the peak while the width continues to decrease. At even larger  $t_w$ , the Raman population at all energies decreases until becoming approximately zero when the bandwidth of the laser is too narrow to allow any change in energy. As

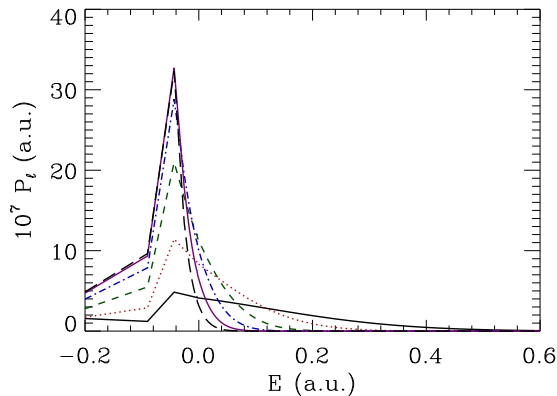


FIG. 4. (Color online) Same as Fig. 2 but only for  $\ell = 0$  and allowing  $t_w$  to vary as in Fig. 3:  $t_w = 6$  a.u. (solid line), 10 a.u. (dotted line), 15 a.u. (dashed line), 20 a.u. (dash-dotted line), 25 a.u. (dash-dot-dot-dotted line), and 30 a.u. (long-dashed line). The longer duration gives a narrower energy distribution. The probability to be in the states nearest  $n = 2$  increases with increasing duration until the bandwidth of the laser becomes too narrow to reach those states.

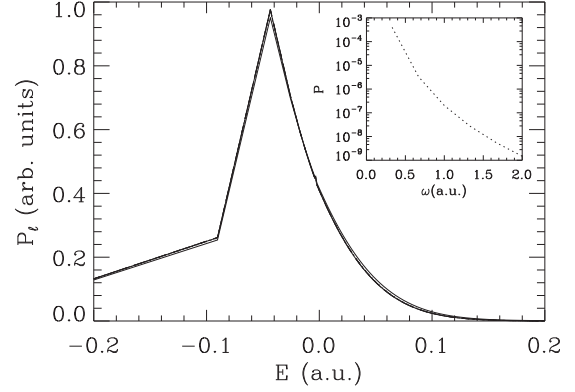


FIG. 5. Same as Fig. 4 but fixing  $t_w = 18$  a.u. and allowing  $\omega$  to vary. The integrals of the curves have been fixed to be the same value. The curves are  $\omega = 0.33$  a.u. (solid line), 0.67 a.u. (dotted line), 1.0 a.u. (dashed line), 1.33 a.u. (dash-dotted line), 1.67 a.u. (dash-dot-dot-dotted line), and 2.0 a.u. (long-dashed line). The lines are hardly distinguishable even though the total Raman probability decreases by more than four orders of magnitude from  $\omega = 0.33$  to 2.0 a.u. This shows that the shape of the energy distribution mainly depends on the laser duration and, hence, the shape of the hole does not strongly depend on the laser frequency. Inset: The total population in the  $\ell = 0$  Raman transition vs the laser frequency.

with Fig. 2, populations in individual states are hard to visualize. The population in the  $1s$  state for each of the curves ( $t_w = 6$ –30 a.u.) is  $1.46 \times 10^{-7}$ ,  $3.95 \times 10^{-8}$ ,  $1.08 \times 10^{-9}$ ,  $4.35 \times 10^{-12}$ ,  $1.87 \times 10^{-15}$ , and  $1.87 \times 10^{-19}$  while the population in the  $3s$  state is  $1.67 \times 10^{-8}$ ,  $4.02 \times 10^{-8}$ ,  $7.62 \times 10^{-8}$ ,  $1.09 \times 10^{-7}$ ,  $1.30 \times 10^{-7}$ , and  $1.34 \times 10^{-7}$ .

Figure 5 shows how the energy distribution for the  $\ell = 0$  Raman transition changes as the *frequency* changes keeping the pulse duration at  $t_w = 18$  a.u. The shape of the energy distribution is nearly the same for all frequencies shown even though there is a difference of more than five orders of magnitude in the total population. This fits with the interpretation of “hole burning” since the shape of the hole will mainly depend on the duration of the pulse and only weakly on the laser frequency; the Raman transitions arise from the projection of the hole in the initial wave function onto neighboring states. We note that the central energy of the two-photon absorption peak shifts by  $\sim 10/3$  a.u. for the same range of frequencies shown in Fig. 5 because the energy of the two-photon peak is at  $\simeq E_g + 2\omega$ .

Figure 6 shows that the Raman transition is related to the duration of the pulse but is *not* directly related to the bandwidth of the laser pulse. This figure shows two different two-photon processes (two-photon absorption and Raman) with the resulting energy distribution. There are three calculations with parameters chosen to disentangle the effect of laser bandwidth from laser duration. To do this, we performed a calculation with a laser chirp. We modified Eq. (3) so that the sin term becomes  $\sin(\omega_0 t + \phi + \eta t^2/t_w^2)$  where  $\eta$  is a measure of the laser chirp. Two pulses will have the same bandwidth if  $\sqrt{1 + \eta^2}/t_w$  are the same. In Fig. 6, the dotted curve has  $t_w = 6, \eta = 0$ ; the dashed curve has  $t_w = 30, \eta = 0$ ; and the solid curve has  $t_w = 30, \eta = \sqrt{24}$ . Thus, the solid curve corresponds to a laser with the same duration of the

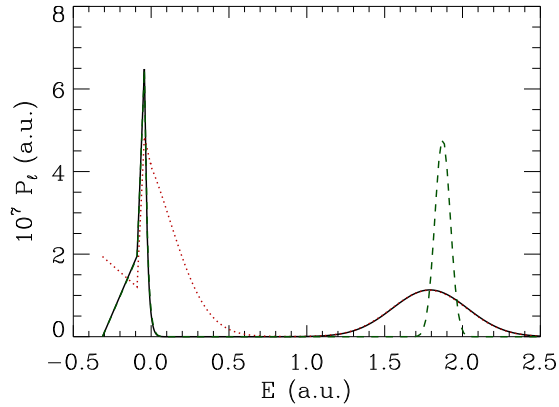


FIG. 6. (Color online) The  $\ell = 0$  energy distribution for  $\omega = 1$  a.u. and  $F_{\max} = 0.05$  a.u. The dotted line is for an unchirped  $t_w = 6$  a.u. pulse; the dashed line is for an unchirped  $t_w = 30$  a.u. pulse with the height scaled by a factor of 0.2 to account for the  $5 \times$  greater fluence. The solid line is for a  $t_w = 30$ -a.u. pulse chirped with  $\eta = \sqrt{24}$ . This chirp gives the same spectral width as the  $t_w = 6$ -a.u. pulse (i.e., converting the chirped pulse to a Fourier-transformed limited pulse would give the 6-a.u. pulse). The height of the chirped pulse is multiplied by 0.214 to match the two-photon absorption of the unchirped 6-a.u. pulse.

dashed curve but it has the bandwidth of the dotted curve. Note that the two-photon absorption for the chirped pulse almost perfectly overlaps the two-photon absorption of the unchirped 6-a.u. pulse, showing that the two-photon absorption depends on the bandwidth while the Raman transition for the chirped pulse almost perfectly overlaps the Raman transition for the unchirped 30-a.u. pulse, showing the Raman transition depends on the duration.

The results in Fig. 6 are directly predicted from hole burning in the initial state. A possible way of understanding how this might result is to examine the difference in two-photon absorption versus photon absorption followed by photon emission. For one-photon absorption, the time dependent term in the Hamiltonian looks like  $\exp[-(t/t_w)^2 + i(\omega_0 t + \phi + \eta t^2/t_w^2)]$ . The emission term is the complex conjugate of the absorption term. For two-photon absorption, the time dependent phases add, which will lead to a central energy at  $E_g + \omega_0 + \omega_0$  with a bandwidth twice that of one-photon absorption. For photon absorption and photon emission, the time dependent phases cancel, which will lead to a central energy at  $E_g + \omega_0 - \omega_0 = E_g$  with a bandwidth only determined by the duration  $t_w$ .

We performed calculations for other single valence atoms and found similar results. An exception is when the single-photon transition is at a Cooper minimum. The single-photon ionization is strongly suppressed in this situation while the two-photon absorption is enhanced compared to the Raman transition.

#### IV. ONE- and THREE-PHOTON IONIZATION

The “hole burning” can affect the one-photon absorption process by changing the time when the electron is ionized and by changing the energy distribution near the one-photon absorption peak. Within a perturbative picture, these effects result from the interference between one-photon absorption

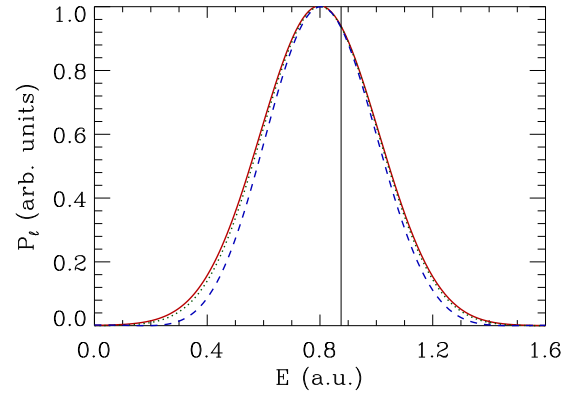


FIG. 7. (Color online) Same as Fig. 2 but for  $\ell = 1$  and allowing  $F_{\max}$  to vary; the graph shows  $F_{\max} = 0.2$  (solid line), 0.4 (dotted line), and 0.8 a.u. (dashed line). The maximum value has been set to 1 for all curves. The energy distribution for the highest laser intensity is narrower and is slightly shifted to higher energies. The vertical line marks the energy  $E_{\text{init}} + \omega$  where a narrow-band laser would give the one-photon ionization.

and a three-photon process (absorb-emit-absorb). The effect of “hole burning” should be to delay the photon absorption because the wave function is being depleted near the nucleus, which is where photoabsorption takes place; the photoabsorption is delayed for strong laser fields because the electron probability near the nucleus needs to refill, which requires time. Unlike the Raman process, which is present even for weak laser fields, this effect should only become apparent at higher laser intensity reflecting a substantial change in the wave function.

For this section, we fixed the duration,  $t_w = 6$  a.u., and frequency,  $\omega = 1$  a.u., of the laser pulse. In all calculations, we started from the  $2s$  state of hydrogen. The general trends did not depend strongly on the type of atom or initial state.

Figure 7 shows the energy distribution for  $\ell = 1$  near the one-photon absorption peak for  $F_{\max} = 0.2, 0.4,$  and  $0.8$  a.u. These fields correspond to intensities of  $1.4 \times 10^{15}$ ,  $5.6 \times 10^{15}$ , and  $2.2 \times 10^{16}$  W/cm<sup>2</sup>. The maxima have been scaled to equal 1 for all  $F_{\max}$ . As with the two-photon absorption peak in Fig. 2, the position of the peak,  $\approx 0.8$  a.u., is slightly shifted to lower energy compared to the expected value:  $1 - 1/8 = 0.875$  a.u., which is marked by a vertical line. The explanation of the shift is the same: the dipole transition matrix element is a decreasing function of energy. While the smaller  $F_{\max}$  have nearly the same shape, the energy distribution is narrower and shifted slightly higher for the  $F_{\max} = 0.8$ -a.u. case. This effect must be due to the interference between one-photon absorption and a three-photon process (either emit-absorb-absorb or absorb-emit-absorb or absorb-absorb-emit). By scaling all curves to have a peak of 1, we are hiding the fact that the energy distribution increases with laser intensity. The ionization probability versus  $F_{\max}$  is not quadratic over this range; the values for  $(F_{\max}, P_{\text{ion}})$  are  $(0.05, 3.76 \times 10^{-4})$ ,  $(0.1, 1.50 \times 10^{-3})$ ,  $(0.2, 5.94 \times 10^{-3})$ ,  $(0.4, 2.28 \times 10^{-2})$ , and  $(0.8, 7.86 \times 10^{-2})$ . In Fig. 7, the ratio of scaling factors for the highest and lowest intensities was 12 instead of 16, which is expected from lowest-order perturbation theory.

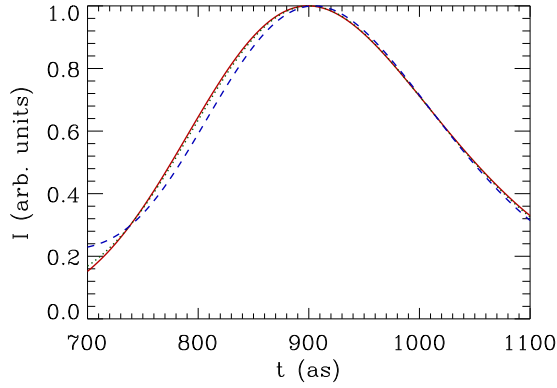


FIG. 8. (Color online) The electron current at  $r = 50$  a.u. from all angular momenta; the line types have the same meaning as Fig. 7. All the times shown are after the laser field is off. Note that the current at the highest intensity has slightly shifted to later times, which agrees with the expectation of changes due to “hole burning”.

As a point of comparison for the largest  $F_{\max}$ , we compared other processes to that shown in Fig. 7. The  $p$ -wave three-photon absorption is 240 times smaller. The  $f$ -wave energy distribution is approximately 1000 times smaller for three-photon absorption and 2000 times smaller for the  $f$ -wave peak near 0.8 a.u. These small values might be surprising compared to the large nonperturbative character for the “one-photon” peak (e.g., the one-photon absorption was approximately 25% too small at  $F_{\max} = 0.8$  a.u.). However, it must be remembered that the three-photon processes can interfere with the one-photon process, which can lead to a larger effect: the probability for an effect arising from interference of one- and three-photon transitions is  $P = |A_1 + A_3|^2 = |A_1|^2 + (A_1 A_3^* + A_1^* A_3) + |A_3|^2$ . The interference term is proportional to the square of the laser intensity while pure three-photon processes are proportional to the cube of the laser intensity; an  $|A_3|$  that is 10%  $|A_1|$  gives the approximate change to the “one-photon” absorption peak and the approximate size of the three-photon absorption peak. We note that the energy spread for the three-photon absorption peak is  $\sim 50\%$  broader than the one-photon peak; the extra broadness arises because the higher-order process depend on higher powers of the intensity and, thus, they appear to be effectively shorter in duration. A simplistic argument would suggest that the one-photon peak would get broader at higher intensity because of the addition of three-photon character. The narrowing we actually observe must be due to interference.

Figure 8 shows the time dependent current at  $r = 50$  a.u. with the peak of the current scaled to be 1. A simple estimate of when the current should peak is  $t_{\text{peak}} \sim 50/\sqrt{2E} = 39.5$  a.u.  $\simeq 953$  as. The actual peak is somewhat earlier in time because the  $-1/r$  potential gives a higher radial speed to the electron; a classical electron with energy 0.8 a.u. requires 907 as to reach 50 a.u. The time required for the electron to reach  $r = 50$  a.u. for the nonhole burning case has been discussed in many different contexts; see Ref. [14] for a recent discussion of time delays in attosecond experiments. As in Fig. 6, the smaller intensities give similar results while the highest intensity gives a clear change. Part of the change is the current due to two-photon absorption, which leads to higher-energy electrons and

a peak at early times; in a similar vein, there is a slow decay at the highest intensity due to the Raman process, which gives low-energy electrons that reach  $r = 50$  a.u. at later times. A more interesting effect is that the one-photon peak is delayed by  $\simeq 6$  as. Quantum mechanically this effect is due to the interference between one- and three-photon paths. Physically, the effect is consistent with the expectation of a time delay due to hole burning in the wave function.

We note that the interference between one- and two-photon processes in a single attosecond absorption has been discussed for both energy and angular distributions. Reference [15] discussed the effect on electron asymmetries, Ref. [16] discussed the effect on momentum and energy distributions, and Ref. [17] gave an analysis based on perturbation theory. In our Fig. 2, one can see that the one-photon absorption peak which falls between the Raman and two-photon absorption peak would overlap them in energy. This would lead to left or right asymmetries in the electron angular distribution as discussed in Ref. [15].

## V. CONCLUSIONS

We have performed calculations of attosecond absorption in one electron systems to explore some of the possible two- and three-photon effects. Our calculations demonstrate that one of the main two-photon effects is a Raman type process that leads to a strong redistribution of population with the same angular momentum as the initial state. We expect this process to be common and related to “hole burning” of the initial wave function. The calculations also show that the interference of one- and three-photon paths can lead to changes substantially larger than might be expected. We argued that the time delay in the one-photon absorption with increasing laser intensity is also due to “hole burning” of the wave function [9]. Because the absorption mainly occurs near the nucleus, a hole there will decrease the ionization rate and lead to a delay of the photoabsorption.

In this paper, we focused on the hole burning in a one electron system. There can be other types of hole burning in two (or more) electron systems. An example involving a short-range perturber coupled to a Rydberg series was investigated using the Ba  $6snd\ ^{1,3}D_2$  states perturbed by the  $5d7d\ ^1D_2$  state as the example [10,18]. As an example requiring attosecond lasers, the Be ground state is nominally  $2s^2$  in the valence shell. Calculations that include correlation have found that there is a large admixture of  $2p^2$  in the ground-state wave function. Typically, the photoionization is different from  $2s$  and  $2p$  orbitals. This leads to the possibility of having a hole burned in the radial coordinate (as described above) and a hole burned in the correlation. This will lead to substantial Raman transition to the nominally  $2p^2$  autoionizing state. Thus, other types of wave packets can be initiated using hole burning.

## ACKNOWLEDGMENTS

This work was supported by the Chemical Sciences, Geosciences, and Biosciences Division of the Office of Basic Energy Sciences, US Department of Energy and by Netherlands Organization for Scientific Research (NWO). We acknowledge support from the European Union Marie Curie Initial Training Networks COHERENCE Network.

- [1] P. M. Paul *et al.*, *Science* **292**, 1689 (2001).
- [2] M. Schultze *et al.*, *Science* **328**, 1658 (2010).
- [3] K. Klunder *et al.*, *Phys. Rev. Lett.* **106**, 143002 (2011).
- [4] D. Guenot *et al.*, *Phys. Rev. A* **85**, 053424 (2012).
- [5] S. Nagele, R. Pazourek, J. Feist, and J. Burgdorfer, *Phys. Rev. A* **85**, 033401 (2012).
- [6] U. Fano, *Phys. Rev. A* **32**, 617 (1985).
- [7] Using the stationary phase argument of Ref. [6], the main accumulation of the matrix element occurs when the initial and final radial momenta are approximately equal. This is only possible if  $\ell$  increases (decreases) when a photon is absorbed (emitted), which Ref. [6] characterized as a propensity rule. The value  $r \sim \sqrt{(\ell+1)/\omega}$  is derived by setting the radial momentum for angular momentum  $\ell+1$  and energy  $E_{\text{gnd}} + \omega$  equal to the initial radial momentum for angular momentum  $\ell$  and energy  $E_{\text{gnd}}$ .
- [8] L. D. Noordam, H. Stapelfeldt, D. I. Duncan, and T. F. Gallagher, *Phys. Rev. Lett.* **68**, 1496 (1992).
- [9] J. H. Hoogenraad, R. B. Vrijen, and L. D. Noordam, *Phys. Rev. A* **50**, 4133 (1994).
- [10] D. I. Duncan and R. R. Jones, *Phys. Rev. A* **53**, 4338 (1996).
- [11] T. Topcu and F. Robicheaux, *J. Phys. B* **40**, 1925 (2007).
- [12] F. Robicheaux, *J. Phys. B* **45**, 135007 (2012).
- [13] The way we grouped the Raman and two-photon absorption is not accurate for  $t_w$  smaller than the data shown because the two-photon absorption begins to have probability below  $E = 0.875$  and the Raman transition has probability above  $E = 0.875$ .
- [14] J. M. Dahlstrom, A. L'Huillier, and A. Maquet, *J. Phys. B* **45**, 183001 (2012).
- [15] L.-Y. Peng, F. Tan, Q. Gong, E. A. Pronin, and A. F. Starace, *Phys. Rev. A* **80**, 013407 (2009).
- [16] L.-Y. Peng, E. A. Pronin, and A. F. Starace, *New J. Phys.* **10**, 025030 (2008).
- [17] E. A. Pronin, A. F. Starace, M. V. Frolov, and N. L. Manakov, *Phys. Rev. A* **80**, 063403 (2009).
- [18] R. B. Vrijen, J. H. Hoogenraad, and L. D. Noordam, *Phys. Rev. A* **52**, 2279 (1995).